Novel Subcooled Boiling Chamber With Submerged Condensation for High Heat Flux Removal for Data Center Application

Maharshi Y. Shukla
Department of Mechanical Engineering,
Rochester Institute of Technology,
Rochester, NY, U.S.A.
Email: ms1235@rit.edu

Satish G. Kandlikar*
Department of Mechanical Engineering,
Rochester Institute of Technology,
Rochester, NY, U.S.A.
Email:sgkeme@rit.edu

*Corresponding Author
Satish G. Kandlikar
Department of Mechanical Engineering, Rochester Institute of Technology, 76 Lomb Memorial Drive, Rochester, NY, 14623, U.S.A.
E-mail: sgkeme@rit.edu,
Telephone: +1-(585)-475-6728
Fax: +1-(585)-475-6879

***Abstract*— Electronic components, especially the CPUs/GPUs used in data centers are concentrated heat-generating sources. Their large Thermal Design Power (TDP), small die area and confined packaging make their thermal management a unique challenge. While conventional single-phase cooling methods fail to dissipate such large amounts of heat efficiently, recently developed two-phase cooling systems also lack the holistic approach of combining efficient boiling and condensation mechanisms. It is hypothesized that subcooled boiling with submerged condensation and reduced saturation pressure will result in high-heat flux dissipation while maintaining low surface temperatures. The novel boiling chamber presented in this work is demonstrated in a compact configuration that fits in a 1U/2U server rack by combining submerged condensation with subcooled pool boiling. The boiling chamber is filled with 13% and 40% fill ratio of water and Novec-7000 and experimentally investigated on a thermal test vehicle. Results show that the boiling chamber dissipates about 400 W of heat with a surface temperature of less than 80 °C using Novec-7000 working fluid. When tested with water, the device dissipated more than 750 W of heat (heat flux ≈ 67 W/cm^2) with a surface temperature of less than 90 °C. Though the surface temperature rose to 120°C, further testing shows the device to dissipate more than 1 kW from a 34.5 × 32 mm^2 plain copper chip. High-speed images identify submerged condensation and small diameters of vapor bubbles. Further enhancements can be achieved by implementing enhanced boiling and condensation surfaces. Lastly, a guide to design considerations and future work is provided to unlock the greater performance potential of the novel boiling chamber.**

Keywords*— data center cooling, electronics cooling, submerged condensation, subcooled boiling, heat transfer, HFE-7000

I. INTRODUCTION

Over the past few years, the amount of data transferred through the internet and the number of internet users has significantly increased [1]. More data centers are being built to cater to the anticipated rising demand from artificial intelligence (AI) technology, and increasing their energy consumption contributes to more than 3% of the global demand. However, more than 30% of the energy consumption in a data centre is used to cool the components and the data center itself [2]. Additionally, computing frameworks like edge computers [3] and cloud computers [4] employ Accelerated Processing Units (APUs) [5], and Graphical Processing Units (GPUs) [6] that can have a Thermal Design Power (TDP) of over 700 W. These high-performing electronic components serve as concentrated heat sources that need to be maintained below a certain temperature for their safe and continual operation.

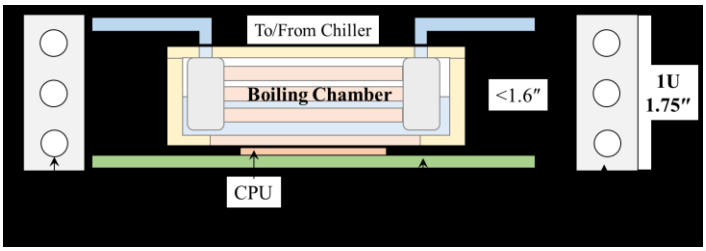

Figure 1. Conceptual schematic of the novel Boiling Chamber CPU cooler in a 1U server rack.

Data centers and server rooms are installed with racks of server boards. The dimensions of these server boards range from 1U to 7U, where U is equivalent to 1.75″ of headspace. High-density data centers aim to package racks with 1U servers to maximize computing power in less space. Thermal management of such data centers is usually taken care of by Chiller Room Air Conditioning (CRAC) systems [7]. These CRAC systems work by circulating cold air across the data center to collect heat [7]. While it has served the cooling needs so far, the fundamental system design and the poor thermal properties of air inhibit efficient (low junction temperature) and effective (high CHF in

a boiling system) heat dissipation. Other device-level cooling techniques like the thermosiphon loop [8], heat pipe-based systems [9], immersion cooling [10], and water cooling [11] are some of the possible solutions, but they have several shortcomings. The thermosiphon-based systems are restricted by the gravity head, the heat pipe-based systems are restricted by surface dryout at higher heat loads, the immersion cooling requires a large amount of dielectric working fluid, and the water cooling systems encounter large pressure drops. In addition, the severe space limitations imposed by the 1U/2U servers require the heat-dissipating device to have a compact configuration. Therefore, a solution that can effectively dissipate a high amount of heat while keeping a low surface temperature in a compact configuration is highly desirable.

Two-phase heat transfer has proven to dissipate high-heat fluxes in electronics cooling. However, the heating surface needs to heat up to the saturation temperature of the working fluid at least before the benefits can be reaped. Options like using a working fluid with a low boiling point, like the 3M Novec 7000, or reducing the saturation pressure form attractive alternatives to reduce surface temperature. However, integrating an efficient condensing mechanism is essential to sustain boiling heat transfer and device performance. Subcooling liquid in a submerged condenser configuration will provide a dual enhancement in condensation and boiling processes.

Subcooled pool boiling is a phenomenon wherein the liquid bulk is maintained at a temperature below the saturation temperature. The subcooled liquid bulk also enables efficient condensation of nucleating vapor bubbles detaching from the heater surface. Subcooling liquid bulk creates an intricate connection between subcooled boiling and submerged condensation. It has been found that bulk liquid subcooling and vapor condensation can also be accomplished through direct contact cooling [12]. Moreover, subcooled pool boiling is proven to advantageous to reduce vapor bubble diameter and delay bubble crowding and Critical Heat Flux (CHF) [13].

For submerged condensation, recent numerical and experimental studies have analyzed vapor condensation in the subcooled liquid and show strong relations between decreasing vapor bubble diameter and increasing liquid subcooling [14–16]. These observations are validated through experiments performed on small heaters at varying gravity and subcooling conditions [17].

Elkassabgi and Lienhard found that at lower subcooling, maximum heat flux dissipation increases linearly with increasing subcooling, but at higher subcooling, the maximum heat transfer is not limited by energy removal rate [18]. Subcooled pool boiling is particularly useful for enhancing the heat dissipation capacity of dielectric refrigerants. El-Glenk and Pourghasemi found CHF to increase from 31 W/cm^2 to 39 W/cm^2 upon increasing Novec 7000 subcooling from 0 K to 15 K [19]. Similar CHF enhancement with HFE-7100 and FC-72 was noted by El-Glenk and Parker [20,21]. However, increasing subcooling is also linked to a delayed transition from natural convection to nucleate boiling [22]. Therefore it is hypothesized that coupling subcooled boiling with submerged condensation can devise a compact cooling system that can fit in 1U and 2U server racks while being capable of dissipating a high amount of heat and keeping a low surface temperature. Kandlikar and Shukla submerged a condensing coil partially in the liquid region and proposed a boiling chamber for high-flux dissipation of heat from CPUs/GPUs while maintaining a low surface temperature [23]. Current work investigates the thermal performance of the novel boiling chamber proposed by Kandlikar and Shukla [23]. Figure 1 shows a conceptual schematic of the compact novel boiling chamber fit in a 1U server rack.

The present work presents a novel boiling chamber to dissipate heat from individual CPUs packed in 1U and 2U server racks. The novel boiling chamber uses subcooled boiling and submerged condensation to achieve high-heat flux dissipation in a compact packaging. The total heat dissipation is experimentally investigation using the boiling chamber with a 13% and 40% fill ratio of water and Novec 7000 over a plain copper test chip. Thermal performance is analyzed using theoretical heat transfer calculations, and high-speed imaging is used to record vapor bubble movement and reveal the underlying heat transfer mechanisms. Moreover, design considerations and future directions are suggested can guide making the boiling chamber more compact and capable.

II. Research Method

Current work presents a novel boiling chamber that can fit in a compact server rack and cool CPUs. The device is experimentally tested on a thermal test vehicle to dissipate high-heat flux through subcooled boiling and submerged condensation. The following sections describe the apparatus, experimental procedure, data acquisition system, and theoretical equations used for generating the results.

A. Test Chip

The test chip acts as a heat spreader and conducts heat from the heat source to the active boiling surface. The test chip is made of Copper 101 alloy having a thermal conductivity of 391 W/(m-K). A schematic of the plain copper chip in the present study is shown in Fig. 2.

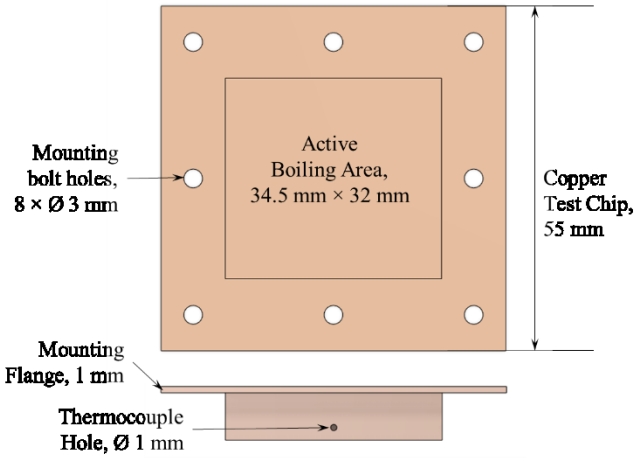

Figure 2. Schematic of plain copper test chip used as the active boiling surface in the experimental investigation.

It is seen from Fig. 2 that the exterior dimension of the copper test chip is 55 mm × 55 mm. The chip has an active boiling surface area of 34.5 mm × 32 mm in the center. The top surface of the test chip has a thickness of 1 mm, and a stem with a cross-sectional area equal to the active boiling area extends 7.5 mm from the base of the heater surface. A 1 mm hole is drilled on one of the 32 mm wide faces of the stem to accommodate a thermocouple hole for recording temperatures during the experiments. An average roughness of 3.2 µm was measured on the plain active boiling surface. The Active boiling area is referred to the region on the plain copper chip where vapor bubble nucleation occurs. The area outside of the active boiling area is taped with Kapton tape before securing the copper chip to the boiling chamber with eight mounting bolts. Kapton tape prevents heat transfer and boiling on the surface outside of the active boiling area.

B. *Experimental Setup*

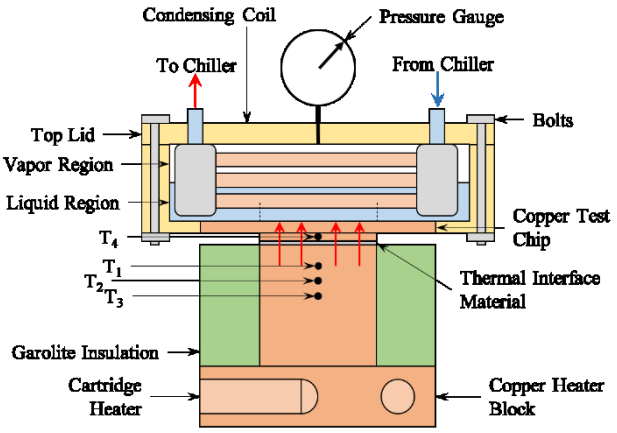

Figure 3. Schematic of the novel subcooled boiling chamber testing assembly.

The experimental setup consists of the following five major components: the boiling chamber, power supply, data acquisition system, high-speed camera, and chiller unit. Schematic of the boiling chamber assembly is shown in Fig.3 and a schematic of the experimental setup is shown in Fig. 4.

The boiling chamber is an assembly of a condenser packaged in an aluminum housing with a transparent polycarbonate lid. The plain copper test chip described in the previous section is bolted at the bottom of the boiling chamber. The chamber is connected to a pressure gauge to measure the system pressure, a thermocouple to measure the working fluid pool temperature, and a charging-discharging port to fill the boiling chamber with the desired amount of working fluid. The assembled boiling chamber has a volume of approximately 150 ml, and for the present study, 20 ml (13% fill) and 60 ml (40% fill) of working fluid is charged into the system. In both configurations, the condenser coil was partly submerged in the liquid pool approximately in proportion to the fill ratio. The condenser is made using a bundle of nine 0.25″ outer diameter and 50.5 mm long copper tubes running from the inlet port to the return manifold and from the return manifold to the outlet port. The total condensing surface area on the condenser is more than 27,000 mm^2. The inlet and outlet ports of the condenser located in the chamber are connected with a chiller using thermocouple-embedded union couplers. The boiling chamber assembly is then brought into contact with a copper heater block. Arctic Silver MX-5 thermal interface material is applied between the top surface of the copper heater block and the bottom of the copper test chip according to the manufacturer's instructions. The thermal interface material primarily constituents of Aluminum and has a thermal conductivity of 4 W/mK.

The copper heater block acts as a thermal test vehicle and is machined from copper 101 alloy. It houses four 400 W cartridge heaters and conducts the heat from the cartridge heaters to the heater chip. The heater block has three holes drilled 5 mm apart for inserting T_1, T_2, and T_3 thermocouple probes. These thermocouples are used for calculating the heat supplied to the boiling chamber. The T_4 thermocouple slid into the copper test chip and is used for measuring temperature and surface temperature calculations in the copper test chip. A garolite insulation sleeve is wrapped around the heater block stem to reduce heat loss. The boiling chamber and copper heater block assembly are held together with spring-loaded aluminum top and bottom plates. Lastly, a vacuum pump is connected to the charging/discharging port for degassing and depressurizing before hermetically sealing the boiling chamber.

Four different boiling chamber configurations have been experimentally studied and their performance is compared. The four configurations are: 13% fill ratio with Novec-7000, 40% fill ratio with Novec-7000, 13% fill ratio with water, and 40% fill ratio with water.

C. *Experimental Procedure*

After assembling, charging, and creating a vacuum, the boiling chamber assembly is connected to the heater section and condenser coils. Then, a chiller is connected to the condenser coil situated in the boiling chamber and set to the desired temperature to flow chiller water through the condensing coil at a flowrate of 2.6 L/min. The thermocouples are connected to a custom National Instruments (NI) LabVIEW program using the NI cDAQ 9172 chassis and NI 9211 module. Thereafter, the cartridge heater leads are plugged with a voltage-controlled power source. The high-speed camera is turned on and the field of view is set to look down on the heater surface. Once the

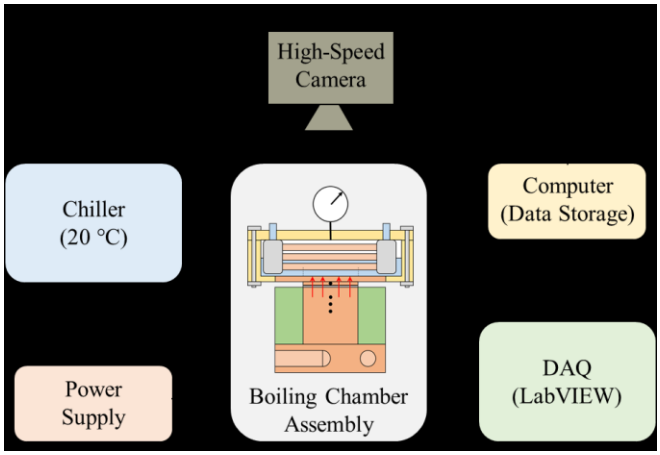

Figure 4. Schematic of the experimental setup showing boiling chamber assembly connected with major components.

apparatus is connected, the experiment is started by setting the power source at 20 V supply, causing the onset of nucleate boiling. With an increasing heat supply, the temperature rise is monitored using the LabVIEW program and measurements are recorded when the system reaches a steady state. Pressure, temperature, and high-speed videos at 500 FPS are recorded at each data point. Data points are recorded at an increment of 3 V until the system reaches CHF, exceeds 100 kPa gauge pressure, or the power source reaches the maximum supply of 1200 W. In case of reaching CHF, the power supply to the cartridge heater is cut off to prevent equipment damage.

D. Heat Transfer Calculation

The theoretical heat transfer analysis conducted in the present work includes calculating heat flux, heat load, surface temperature, and thermal resistance. The procedure adopted is similar to previously published work available in the literature [24,25].

Heat flux supplied through the copper heater block is calculated using Fourier's 1D conduction law. Equation 1 shows the formula used to calculate the heat flux.

$$q'' = -k_{Cu}\frac{dT}{dx} \quad (1)$$

Where q'' is heat flux in W/cm^2, k_{Cu} is the thermal conductivity of copper, and dT/dx is the temperature gradient calculated from the temperature recorded by T_1, T_2, and T_3 thermocouple probes. The temperature gradient is calculated using Eq. 2.

$$\frac{dT}{dx} = \frac{3T_1 - 4T_2 + T_3}{2\Delta x} \quad (2)$$

Where Δx denotes the spacing of 5 mm between T_1, T_2, and T_3 thermocouple probes. The heat load is then the product of the heat flux dissipated and the boiling area as shown by Eq. 3.

$$Q = q''A \quad (3)$$

Where Q is the heat load dissipated and A denotes the active boiling area, which is equal to 11.04 cm^2. The surface temperature can be calculated using Fourier's 1D conduction law using the calculated flux. The re-arranged Fourier's 1D conduction equation is shown in Eq. 4.

$$T_{sur} = T_1 - q''\left(\frac{x_4}{k_{Cu}}\right) \quad (4)$$

Where T_{sur} is the surface temperature and x_4 denotes a distance of 6.5 mm from the location of the $T4$ thermocouple probe and the active boiling surface. The thermal resistance (R) represents the resistance in the heat flow from the source to the sink and is measured in °C/W.

$$R = \frac{(T_{sur} - T_{sat}) + (T_{sat} - T_{c,i})}{Q} \quad (5)$$

Where T_{sat} is the saturation temperature of the working fluid and $T_{c,i}$ is the temperature of the coolant temperature at the inlet of the condensing coil.

E. Calibration and Uncertainty

Current work uses K-type Omega thermocouples to measure temperature and a Keyence VW-5000E microscope to record high-speed images of the vapor bubbles and boiling regime. While the microscope is pixel calibrated against a known distance and the thermocouples are calibrated in a hot cell, uncertainty in heat flux calculation is calculated using the uncertainty in thermal conductivity of copper, calipers used to measure lengths and thermocouples for temperature measurement. A process similar to previously published work from our research group is employed for thermocouple calibration and uncertainty calculation [8,24]. The uncertainty in a property is calculated using Eq. 6.

$$U_p = \sqrt{\sum_{i=1}^{n}\left(\frac{\partial p}{\partial \sigma_i}U_{\sigma i}\right)} \quad (6)$$

Where p is a property dependent on a variable σ for n samples. The total uncertainty in heat flux calculation is calculated using Eq. 7.

$$\frac{U_{q''}}{q''} = \sqrt{\frac{\left(U_{K_{Cu}}\right)^2}{K_{Cu}^2} + \frac{(U_{\Delta x})^2}{\Delta x^2} + \frac{9\left(U_{T_1}\right)^2}{\alpha^2} + \frac{16\left(U_{T_2}\right)^2}{\alpha^2} + \frac{\left(U_{T_3}\right)^2}{\alpha^2}} \quad (7)$$

Where α is equal to $3T_1 - 4T_2 + T_3$, $U_{K_{Cu}}$ corresponds to uncertainty in the thermal conductivity of copper, $U_{\Delta x}$ is the uncertainty in measuring the distance between adjacent thermocouples, and $U_{T_{1-3}}$ show the uncertainty in temperature measurement from thermocouples T_1, T_2 and T_3. The results reported in the following section are bound in a 95% confidence interval. The uncertainty in heat flux is multiplied by the boiling surface area in the heat dissipation plots.

III. Results

Subcooled pool boiling experiments were conducted using a plain copper heater surface in the boiling chamber. The experiments evaluated the impact of using 20 ml and 60 ml of Novec 7000 and water as the working fluids. The 20 ml of working fluid volume corresponds to about 13% volume filled in the boiling chamber and 60 ml of working fluid volume fills about 40% of the boiling chamber volume. It is to be noted that the percentage of condenser submerged in the liquid region of the working fluid is similar to the percentage of volume occupied by the working fluid in the chamber. The experiments were conducted with a coolant temperature of 20 °C at the inlet of the condenser. The experiments using Novec 7000 were started at a gauge pressure of -40 kPa and the experiments using water were started at a gauge pressure of -90 kPa and the corresponding saturation temperatures are 20 °C and 46 °C, respectively. The experiments were concluded in cases when either CHF was reached or the boiling chamber pressure build-up exceeded 100 kPa gauge pressure.

The following section first compares the heat dissipated by the boiling chamber using 20 ml and 60 ml of Novec-7000 and water, followed by comparing the thermal resistance of the boiling chamber in comparison to other cooling systems, and finally identifies the heat transfer mechanism observed through examining high-speed images of the vapor bubble movement. Moreover, the heat transfer results are compared against air, water, and thermosiphon-based coolers evaluated by Chauhan and Kandlikar [8].

A. Heat Dissipation Analysis

Figure 5 compares the heat load dissipated by the subcooled boiling chamber using 13% and 40% volume fill of Novec 7000. The vertical axis shows the heat dissipation in watts while the

horizontal axis shows the temperature of the heater surface in degrees Celsius. The solid markers signify 40% working fluid fill and the hollow markers show 13% fill.

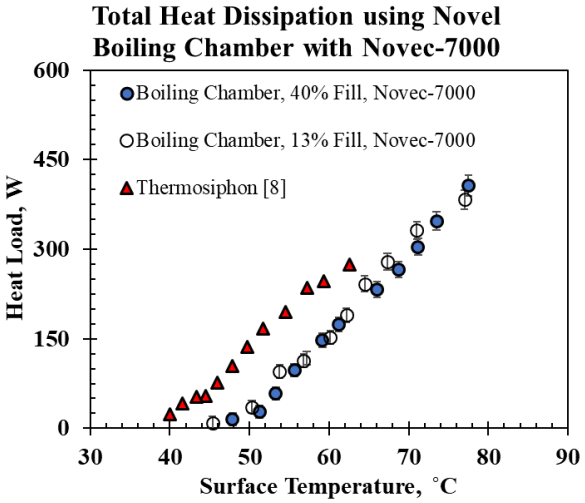

Figure 6. Enhanced heat dissipation using the novel boiling chamber with Novec 7000 at 13% and 40% fill against the dual-taper thermosiphon system developed by Chauhan and Kandlikar [8].

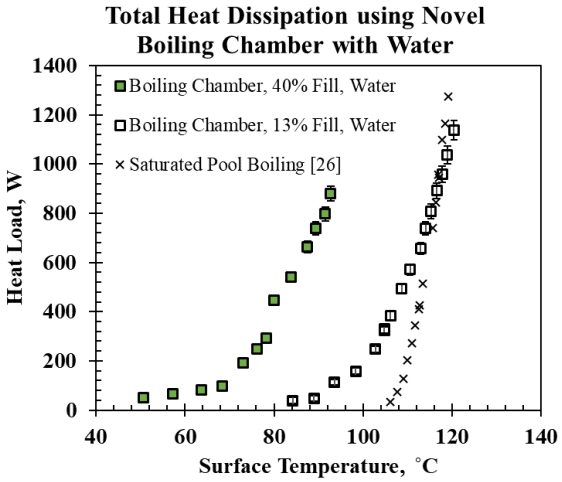

Figure 5. Enabling lower surface temperatures at high heat dissipation using the novel subcooled boiling chamber with water at 13% and 40% fill. The performance is compared against open pool boiling experimental data published by Rishi et al. at 1 atm pressure over plain copper chip with 1 cm^2 and water [26].

It is seen from Fig.5 that the boiling chamber can dissipate about 400 W with 13% and 40% Novec 7000 fill while keeping the surface under 80 °C. The 40% Novec 7000 experiment resulted in a maximum heat dissipation of 406.6 W, equivalent to 36.8 W/cm^2 at a surface temperature of 77.5 °C. The test with 13% water resulted in a 6% lower maximum heat dissipation compared to the experiment with a 40% fill rate. The experiment with 13% fill resulted in a maximum heat dissipation of 383 W (34.7 W/cm^2) at 77 °C. Therefore, increasing the liquid volume enhanced the CHF by 6%, indicating the improvements caused by the submerged condensation process.

Figure 6 compares the heat load dissipated by the subcooled boiling chamber using 13% and 40% volume fill of water with a saturated open pool boiling experiment conducted by Rishi et. al. on a 1 cm^2 plain copper chip [26]. The vertical axis shows the heat dissipation in watts, while the horizontal axis shows the temperature of the heater surface in degrees Celsius. The solid square markers signify 40% working fluid fill, the hollow square markers show 13% fill, and the crosses show the saturated open pool boiling experiment result.

The boiling chamber experiments conducted in the boiling chamber did not reach CHF and were concluded due to the system gauge pressure exceeding 100 kPa. The experiment with 40% water fill in the boiling chamber dissipated about 880.2 W (≈79.7 W/cm^2) at 92.7 °C surface temperature and the experiment with 13% water fill reached a maximum of 1136.6 W (≈102.9 W/cm^2) at a surface temperature of 120 °C. Therefore, the experiment with 20 ml of water yielded a 29.1% higher heat dissipation compared to the experiment with 60 ml of water. However, comparing the heater surface temperature at 880 W of heat dissipation, a 20% reduction in surface temperature with 60 ml of working fluid was observed in comparison to the 20 ml experiment.

The heat flux from the saturated open pool boiling experimental data published by Rishi et al. was multiplied by the active boiling surface area of the plain copper chip used in the current and laid in Fig. 6 [26]. It can be observed that with 13% liquid fill, the boiling chamber functions similarly to a saturated pool boiling system. The similarity can also be justified by the less than 15% immersion of the condenser in the liquid pool. However, with 40% liquid fill, a greater portion of the condensing coil gets immersed in the liquid region, and a lower surface temperature with comparable heat loads is observed. Increasing condenser submersion in liquid bulk enhances subcooling and submerged condensation. The improvement in the condensation process is validated through high-speed images.

B. Thermal Resistance

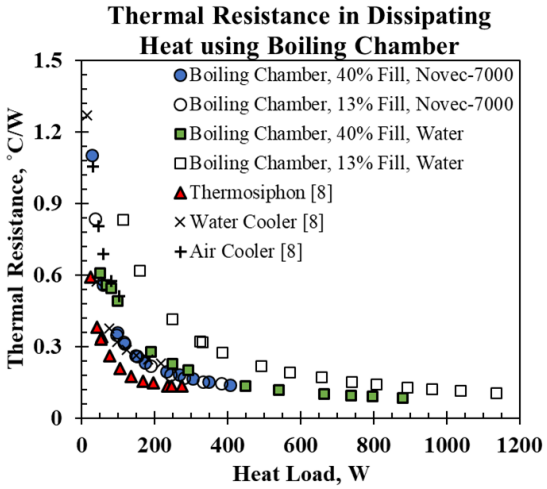

Figure 7. Thermal resistance in dissipating heat from the heater source to the chiller unit using subcooled boiling chamber with Novec-7000 and water at 13% and 40% Fill Rate.

The boiling chamber is conceptualized to provide a device-level, highly capable and efficient thermal management

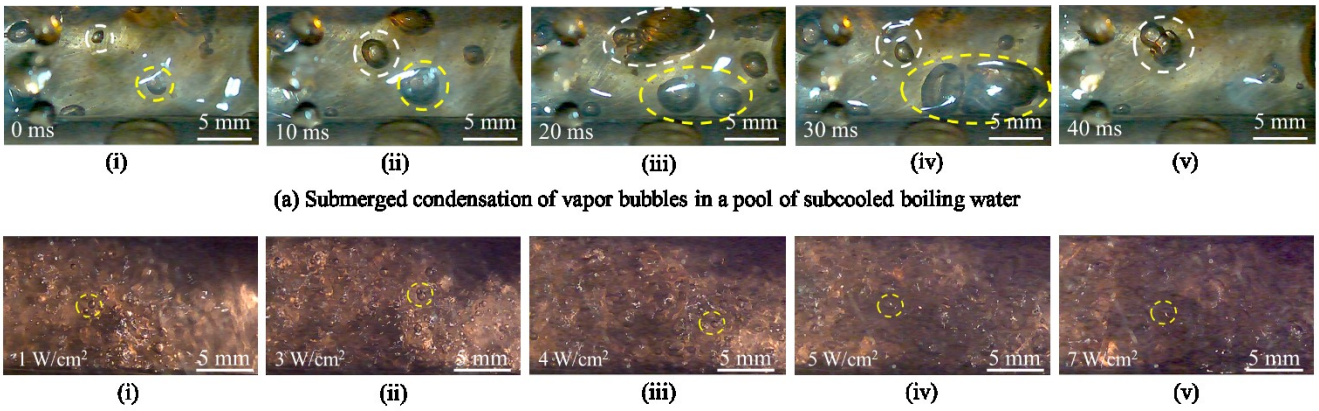

Figure 8. High-speed images of vapor bubble condensation in boiling chamber with 40% liquid fill of Novec-7000 and water. Image sequence (a) shows submerged vapor bubble condensation in subcooled boiling water over plain copper at a heat flux of about 26 W/cm^2. The image sequence (b) shows small and discrete vapor bubbles at varying heat fluxes in a 60 ml subcooled pool of Novec-7000.

solution. Since the system pressure changes through the operation as a function of heat supplied through the copper test chip and the heat dissipated through the condenser, calculating the Heat Transfer Coefficient (HTC) does not provide a true measure of system effectiveness.

On the other hand, comparing thermal resistance in dissipating a unit watt of heat allows comparison with systems using different heat transfer mechanisms. Thermal resistance is calculated as the temperature difference between the surface and the chiller to the unit watt dissipated.

Figure 7 compares the thermal resistance in dissipating heat using the boiling chamber with 13% and 40% volume fill of Novec-7000 and water against the thermal resistance in heat dissipation using thermosiphon, water, and air coolers. The thermal resistance is calculated using the formula given in Eq. 6 and thermosiphon, water, and air cooler experimental data is retraced from Chauhan and Kandlikar [8]. It can be seen from Fig. 6 that compared to water, when using Novec-7000, the boiling chamber can dissipate heat through the boiling chamber with lesser thermal resistance. The lower saturation point enables the Novec-7000 to phase into nucleate boiling sooner than water, but with a thermal conductivity of 8 times greater and significantly higher latent heat, water can dissipate a much larger amount of heat. While the boiling chamber can dissipate heat with lesser resistance compared to a water cooler or air cooler, it could not dissipate heat as efficiently as the thermosiphon loop. However, boiling chamber thermal resistance decreases with increasing heat load and dissipates at least 1.4 times more heat compared to the thermosiphon-based cooler.

When comparing the 13% and 40% fill ratios of Novec-7000 and water in the boiling chamber, it is observed that the 40% fill ratio offers lesser thermal resistance. It is believed that increasing liquid fill increases condenser submersion in the liquid region of working fluid and aggravates submerged condensation. However, when the boiling chamber is filled with 13% fill ratio of water, larger vapor space condensation from lesser submersion of condensing coil enables greater condensation at higher heat loads.

C. Heat Transfer Mechanism

It is evident from the theoretical analysis of the experimental data that the combination of subcooled boiling and submerged condensation can enhance CHF with Novec-7000 and reduce the surface temperature with water. The following section analyzes vapor bubble submerged condensation during the subcooled pool boiling experiments. The high-speed videos were recorded at 500 FPS using a Keyence VW-5000E Motion Analyzer Microscope. Figure 8 shows sequences of high-speed images of vapor bubble condensation in Novec-7000 and water.

Figure 8(a) shows five images of the vapor bubble condensation in a subcooled 60 ml pool of water at an interval of 10 ms. At the bottom of each high-speed image, a scale bar and time stamps are provided for reference. The images are recorded at a heat supply of about 290 W (≈26.4 W/cm^2) with a surface temperature of about 78 °C, saturation temperature of about 60 °C and a liquid bulk temperature of about 55 °C. The white and yellow-bordered circles highlight two bubbles that undergo submerged condensation. The bubble growing inside the white marker undergoes rapid nucleation and expansion in Fig. 8(a)-(i) and Fig. 8(a)-(ii), and starts to condense while detaching in Fig. 8(a)-(iii). However, the bubble does not condense completely while being submerged and leaves a ripple and a nucleate bubble in its wake as seen in Fig. 8(a)-iv, and the cycle continues in Fig. 8(a)-v. In contrast, the bubble marked in yellow undergoes bubble nucleation, expansion, coalescences and complete submerged condensation from Fig. 8(a)-(i) through Fig. 8(a)-(v). The vapor bubble diameter during the experiment conducted with 13% volume fill was comparable to the liquid height, and the bubble formation was similar to the observations of Shukla and Kandlikar [27]. Condensation of these vapor bubbles while coalescence due to direct contact cooling from the condenser enabled higher heat dissipation despite the vapor bubble coalescence forming a foam-like appearance similar to that reported Shukla and Kandlikar [27].

Figure 8(b) shows the high-speed images for subcooled pool boiling in 40% fill of Novec-7000. Figures 8(a)-(i) to 8(a)-(v) show vapor bubble condensation at heat flux increasing from 1 cm^2 to 7 W/cm^2. The pool temperature increased from about 21 °C to 25 °C and the surface temperature increased from 46 °C to 54 °C, while the saturation temperature for these heat fluxes remained close to 34 °C. It is observed from the high-speed images that the vapor bubble diameter remains smaller than 2 mm despite increasing heat dissipation. Increasing the heat flux from 1 cm^2 in 8(b)-(i) to 7 W/cm^2 8(b)-(v) shows increasing vapor bubble density while maintaining a similar bubble diameter. Reduction in vapor bubble diameter due to subcooling in pool boiling is well noted and supplemented in the literature[13–17,28]. Reduction in vapor bubble size is crucial in delaying vapor blanketing, sustaining liquid return to the heater surface, and enhancing CHF. Recent observations from El-Genk and Parker confirm CHF enhancement with subcooled pool boiling with Novec-7000 [19].

IV. Discussion

It is seen from the experimental investigation of the boiling chamber that subcooled boiling and submerged condensation allow the creation of a compact thermal management device capable of high heat-flux dissipation while maintaining a low surface temperature. It is observed that increasing condenser immersion in the liquid region increases subcooling and improves performance by affecting both the submerged condensation and vapor condensation processes. On the one hand, the experiments with water show that with lower liquid fill, the effect of subcooling reduces in the boiling chamber, resulting in a performance similar to saturated pool boiling. On the other hand, the experiments with higher liquid fill show that while increasing liquid fill in the boiling chamber improves submerged condensation, the reduction in vapor region condensation increases saturation pressure and temperature. While submerged condensation is found to be essential in dissipating large amounts of heat from a compact system, the experiment with Novec-7000 at 40% fill highlights the prevailing importance of vapor region condensation. Proper condenser design is expected to overcome this problem by increasing condenser surface area.

A. Comparison of Heat Dissipation

Figure 9 compares the heat transfer performance of the novel boiling chamber to a thermosiphon loop, water cooler and air cooler. The thermosiphon, water cooler and air cooler results is digitized from the work published by Chauhan and Kandlikar [8]. The error bars were not incorporated in the experimental results to avoid clutter in the plot. The horizontal axis shows the heater surface temperature in degrees Celsius, and the vertical axis shows the heat dissipated in watts.

It is seen from the results from Fig. 9 that for a surface temperature of up to 60 °C, the air cooler was able to dissipate just 102 W, the water cooler dissipated 216 W, and the dual taper thermosiphon loop dissipated more than 274 W. In comparison, the boiling chamber can dissipate more than 150 W heat with Novec-7000 and about 80 W heat with water. However, the boiling chamber gets more efficient at higher cooling demands. The boiling chamber dissipates more than 400 W with Novec-7000 while keeping the surface temperature less than 78 °C and 800 W with water while keeping the surface below 90 °C. Moreover, the boiling chamber can dissipate such high heat loads with a plain heater surface whereas the thermosiphon loop result was enhanced by using a microchannel surface and dual-taper microgap.

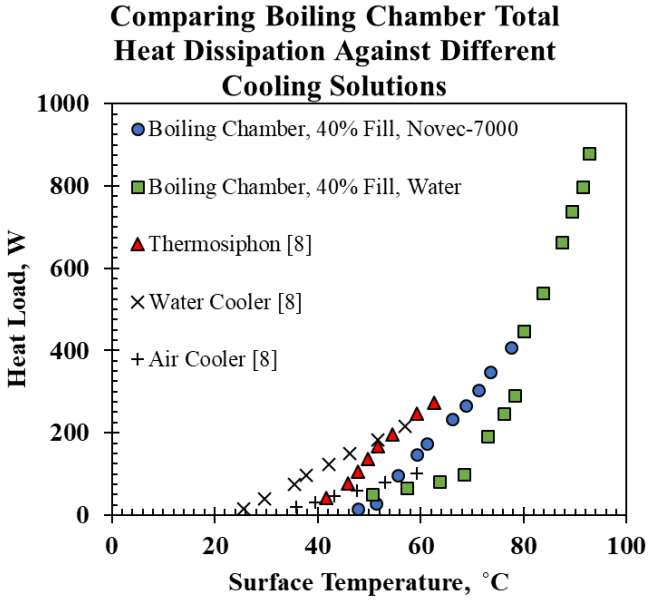

Figure 9. Superior heat dissipation with the novel boiling chamber compared to other solutions. The thermosiphon, water cooler and air cooler data is digitized from Chauhan and Kandlikar [8].

Current work proves that using subcooled boiling and submerged condensation can revolutionize the thermal management strategy adopted for applications with high-heat dissipation from a confined space, especially data center cooling. The following section provides design direction in the creation of products to cool CPUs/GPUs of today and tomorrow in the confines of 1U and 1U servers.

B. Design Consideration

The boiling chamber is an integration of an evaporator and a condenser in compact packaging. The following considerations will help in designing an improvised version.

- Using passive heat transfer enhancement structure on the heater surface to increase evaporator performance
- Employing a working fluid with a low boiling point, high thermal conductivity, dielectric constant, and CHF.
- Condenser geometry that subcools the working fluid promotes submerged condensation, direct contact cooling, and pool agitation without inducing a huge pressure drop on the coolant side.

C. Future Directions

Current work demonstrates the effectiveness of subcooled boiling and submerged condensation through experimental analysis of the boiling chamber using a plain copper chip and a simple condenser design by dissipating more than 1 kW of heat in a package that can fit in a 1U server. Leveraging the extensive research in the literature on enhancing the evaporator and

condenser side performance can dramatically improve the boiling chamber performance.

Using passive heat transfer enhancement techniques through heater surface modifications has resulted in geometries capable of dissipating very large heat fluxes with a meagre increase in wall superheat [29]. Using porous coatings [26], nano-structures [30], re-entrant cavities [31], meshes [32], micro-pillars [33], fins [34], pin-fins [35], microchannels [36], enhanced microchannels [37], grooves [38], buddle diverters [39] can incentivize boiling chamber by enhancing heat transfer, promoting early vapor bubble nucleation, creating additional nucleation sites, establishing separate liquid-vapor pathways, agitating liquid bulk, improving heater surface rewetting [40].

Investigating the effect of different working fluids with the boiling chamber can further aggravate heat dissipation. The impact of thermo-physical properties on heat transfer is well-researched in the literature. Using dielectric refrigerants [41], mineral oils [42] in single-phase configuration, speciality fluids [43], additives [44], nano-fluids [45], and surfactants [46] change the heater-liquid, liquid-vapor, and vapor-condensing surface interactions. Moreover, pool dynamics can be further studied to augment heat transfer mechanisms like microconvection [47], macroconvection [48], transient conduction [49], and microlayer evaporation [50].

Experimental investigation in the current work dictates that improving condenser performance is key to elevating boiling chamber capabilities. A closed system like the boiling chamber will benefit greatly if the heat dissipation capacity of the condenser is greater than that of the evaporator (heater surface) [51]. Besides optimizing the condenser geometry to increase condensation surface area and reduce pressure drop; maximizing chiller water flowrate for any condenser geometry will significantly enhance heat transfer. Moreover, techniques like minichannels [52], microchannels [53], turbulators [54], fins [55], and ribbings [56] can be used to enhance condenser performance for higher high-heat dissipation.

V. Conclusion

To summarize, the present work presents a novel subcooled boiling chamber for dissipating high-heat flux at low surface temperature in a compact packaging capable of fitting in a 1U/2U server rack using subcooled boiling and submerged condensation. Four different boiling chamber configurations have been experimentally studied, and their performance is compared. The four configurations are: 13% fill ratio with Novec-7000, 40% fill ratio with Novec-7000, 13% fill ratio with water, and 40% fill ratio with water. As expected, the boiling chamber experiments with water have a higher heat dissipation rate compared to Novec-7000. However, the Novec-7000 systems are able to provide lower surface temperatures. The performance with 40% fill ratio was higher than 13%, indicating the role of subcooling in the boiling chamber. Further research in this area is being pursued to meet the higher dissipation requirements in the CPUs of future data centers.

The following specific conclusions are drawn from the present study:

- Submerging a condenser partly in the liquid region subcools liquid bulk, allows direct contact cooling and simultaneously augments vapor and submerged condensation.
- Boiling chamber experiment with 13% water fill dissipated more than 1136 W (≈102.9 W/cm^2) of heat with a surface temperature of 120 °C. When the boiling chamber was filled 40% with water, a surface temperature of less than 93 °C was maintained while dissipating more than 880 W/cm^2 (≈79.7 W/cm^2) of heat.
- With Novec-7000 The boiling chamber can dissipate more than 406 W (≈36.7 W/cm^2) of heat at a surface temperature of less than 77 °C with 40% fill ratio and 383 W (≈34.7 W/cm^2) of heat at a surface temperature of less than 77 °C with 13% fill ration.
- High-speed visualization shows that submerged condensation with subcooled pool boiling in water and delayed vapor blanketing with Novec-7000.
- Enhancement mechanisms available in the literature can augment evaporator, bulk, and condenser heat transfer mechanisms.

Optimizing evaporator and condenser geometry can make cooling devices smaller without sacrificing thermal performance.

Acknowledgment

The authors would like to thank Jan Maneti, Rick Wurzer, and Craig Arnold (retired) from the machine shop in the Department of Mechanical Engineering at RIT for machining the parts used for fabricating the novel boiling chamber. The authors would also to thank Noor Mustufa for helping with the design of condenser and Matthew Fuller for help in conducting Novec-7000 experiments.

References

[1] Obringer, R., Rachunok, B., Maia-Silva, D., Arbabzadeh, M., Nateghi, R., and Madani, K., 2021, "The Overlooked Environmental Footprint of Increasing Internet Use," Resources, Conservation and Recycling, **167**, p. 105389.

[2] Li, Z., and Kandlikar, S. G., 2015, "Current Status and Future Trends in Data-Center Cooling Technologies," Heat Transfer Engineering, **36**(6), pp. 523–538.

[3] Cao, K., Liu, Y., Meng, G., and Sun, Q., 2020, "An Overview on Edge Computing Research," IEEE Access, **8**, pp. 85714–85728.

[4] Cheng, H., Liu, B., Lin, W., Ma, Z., Li, K., and Hsu, C.-H., 2021, "A Survey of Energy-Saving Technologies in Cloud Data Centers," J Supercomput, **77**(11), pp. 13385–13420.

[5] Naffziger, S., Beck, N., Burd, T., Lepak, K., Loh, G. H., Subramony, M., and White, S., 2021, "Pioneering Chiplet Technology and Design for the AMD EPYC™ and Ryzen™ Processor Families : Industrial Product," *2021 ACM/IEEE 48th Annual International Symposium on Computer Architecture (ISCA)*, pp. 57–70.

[6] Elster, A. C., and Haugdahl, T. A., 2022, "Nvidia Hopper GPU and Grace CPU Highlights," Computing in Science & Engineering, **24**(2), pp. 95–100.
[7] Patel, C. D., Sharma, R., Bash, C. E., and Beitelmal, A., 2002, "Thermal Considerations in Cooling Large Scale High Compute Density Data Centers," *ITherm 2002. Eighth Intersociety Conference on Thermal and Thermomechanical Phenomena in Electronic Systems (Cat. No.02CH37258)*, pp. 767–776.
[8] Chauhan, A., and Kandlikar, S. G., 2019, "Characterization of a Dual Taper Thermosiphon Loop for CPU Cooling in Data Centers," Applied Thermal Engineering, **146**, pp. 450–458.
[9] Ding, T., He, Z. guang, Hao, T., and Li, Z., 2016, "Application of Separated Heat Pipe System in Data Center Cooling," Applied Thermal Engineering, **109**, pp. 207–216.
[10] Kuncoro, I. W., Pambudi, N. A., Biddinika, M. K., Widiastuti, I., Hijriawan, M., and Wibowo, K. M., 2019, "Immersion Cooling as the next Technology for Data Center Cooling: A Review," J. Phys.: Conf. Ser., **1402**, p. 044057.
[11] Nadjahi, C., Louahlia, H., and Lemasson, S., 2018, "A Review of Thermal Management and Innovative Cooling Strategies for Data Center," Sustainable Computing: Informatics and Systems, **19**, pp. 14–28.
[12] Dhir, V. K., 1998, "Boiling Heat Transfer," Annual Review of Fluid Mechanics, **30**(1), pp. 365–401.
[13] Rainey, K. N., You, S. M., and Lee, S., 2003, "Effect of Pressure, Subcooling, and Dissolved Gas on Pool Boiling Heat Transfer from Microporous, Square Pin-Finned Surfaces in FC-72," International Journal of Heat and Mass Transfer, **46**(1), pp. 23–35.
[14] Hong, S. J., Park, G. C., Cho, S., and Song, C.-H., 2012, "Condensation Dynamics of Submerged Steam Jet in Subcooled Water," International Journal of Multiphase Flow, **39**, pp. 66–77.
[15] Kumar, A., Kangude, P., and Srivastava, A., 2023, "Coupled Bubble Dynamics and Interaction Mechanisms of Adjacently Nucleated Vapor Bubbles under Subcooled Pool Boiling Regime," Physics of Fluids, **35**(8), p. 087107.
[16] Li, S. Q., Wang, P., and Lu, T., 2015, "Numerical Simulation of Direct Contact Condensation of Subsonic Steam Injected in a Water Pool Using VOF Method and LES Turbulence Model," Progress in Nuclear Energy, **78**, pp. 201–215.
[17] Kim, J., Benton, J. F., and Wisniewski, D., 2002, "Pool Boiling Heat Transfer on Small Heaters: Effect of Gravity and Subcooling," International Journal of Heat and Mass Transfer, **45**(19), pp. 3919–3932.
[18] Elkassabgi, Y., and Lienhard, J. H., 1988, "Influences of Subcooling on Burnout of Horizontal Cylindrical Heaters," Journal of Heat Transfer, **110**(2), pp. 479–486.
[19] El-Genk, M. S., and Pourghasemi, M., 2021, "Subcooled Boiling Critical Heat Flux of HFE-7000 Dielectric Liquid on Inclined Rough Cu," International Journal of Heat and Mass Transfer, **175**, p. 121354.
[20] Parker, J. L., and El-Genk, M. S., 2005, "Enhanced Saturation and Subcooled Boiling of FC-72 Dielectric Liquid," International Journal of Heat and Mass Transfer, **48**(18), pp. 3736–3752.
[21] El-Genk, M. S., and Parker, J. L., 2008, "Nucleate Boiling of FC-72 and HFE-7100 on Porous Graphite at Different Orientations and Liquid Subcooling," Energy Conversion and Management, **49**(4), pp. 733–750.
[22] Petrovic, S., Robinson, T., and Judd, R. L., 2004, "Marangoni Heat Transfer in Subcooled Nucleate Pool Boiling," International Journal of Heat and Mass Transfer, **47**(23), pp. 5115–5128.
[23] Kandlikar, S. G., and Shukla, M. Y., 2023, "Cooling Device Having a Boiling Chamber with Submerged Condensation and Method."
[24] Mody, F., Chauhan, A., Shukla, M., and Kandlikar, S. G., 2022, "Evaluation of Heater Size and External Enhancement Techniques in Pool Boiling Heat Transfer with Dielectric Fluids," International Journal of Heat and Mass Transfer, **183**, p. 122176.
[25] Chauhan, A., and Kandlikar, S. G., 2022, "Geometrical Effects on Heat Transfer Mechanisms during Pool Boiling in Dual Tapered Microgap with HFE7000," International Journal of Heat and Mass Transfer, **183**, p. 122165.
[26] Rishi, A. M., Gupta, A., and Kandlikar, S. G., 2018, "Improving Aging Performance of Electrodeposited Copper Coatings during Pool Boiling," Applied Thermal Engineering, **140**, pp. 406–414.
[27] Shukla, M. Y., and Kandlikar, S. G., 2021, "Influence of Liquid Height on Bubble Coalescence, Vapor Venting, Liquid Return, and Heat Transfer in Pool Boiling," International Journal of Heat and Mass Transfer, **173**, p. 121261.
[28] Goel, P., Nayak, A. K., Kulkarni, P. P., and Joshi, J. B., 2017, "Experimental Study on Bubble Departure Characteristics in Subcooled Nucleate Pool Boiling," International Journal of Multiphase Flow, **89**, pp. 163–176.
[29] Kandlikar, S. G., 2013, "Controlling Bubble Motion over Heated Surface through Evaporation Momentum Force to Enhance Pool Boiling Heat Transfer," Appl. Phys. Lett., **102**(5), p. 051611.
[30] Rahman, M. M., Ölçeroğlu, E., and McCarthy, M., 2014, "Role of Wickability on the Critical Heat Flux of Structured Superhydrophilic Surfaces," Langmuir, **30**(37), pp. 11225–11234.
[31] Nakayama, W., Daikoku, T., Kuwahara, H., and Nakajima, T., 1980, "Dynamic Model of Enhanced Boiling Heat Transfer on Porous Surfaces—Part I: Experimental Investigation," Journal of Heat Transfer, **102**(3), pp. 445–450.
[32] Mori, S., and Okuyama, K., 2009, "Enhancement of the Critical Heat Flux in Saturated Pool Boiling Using

Honeycomb Porous Media," International Journal of Multiphase Flow, **35**(10), pp. 946–951.

[33] Duan, L., Liu, B., Qi, B., Zhang, Y., and Wei, J., 2020, "Pool Boiling Heat Transfer on Silicon Chips with Non-Uniform Micro-Pillars," International Journal of Heat and Mass Transfer, **151**, p. 119456.

[34] Yu, C. K., and Lu, D. C., 2007, "Pool Boiling Heat Transfer on Horizontal Rectangular Fin Array in Saturated FC-72," International Journal of Heat and Mass Transfer, **50**(17), pp. 3624–3637.

[35] Bulut, M., Shukla, M., Kandlikar, S. G., and Sozbir, N., 2023, "Experimental Study of Heat Transfer in a Microchannel with Pin Fins and Sintered Coatings," Experimental Heat Transfer, **0**(0), pp. 1–16.

[36] Cooke, D., and Kandlikar, S. G., 2012, "Effect of Open Microchannel Geometry on Pool Boiling Enhancement," International Journal of Heat and Mass Transfer, **55**(4), pp. 1004–1013.

[37] Jaikumar, A., and Kandlikar, S. G., 2016, "Ultra-High Pool Boiling Performance and Effect of Channel Width with Selectively Coated Open Microchannels," International Journal of Heat and Mass Transfer, **95**, pp. 795–805.

[38] Long, J., Liu, Z., Lin, H., Li, Y., Cao, Z., Zhang, Z., and Xie, X., 2022, "Pool Boiling Heat Transfer and Bubble Dynamics over V-Shaped Microchannels and Micropyramids: Does High Aspect Ratio Always Benefit Boiling?," Applied Thermal Engineering, **201**, p. 117796.

[39] Chauhan, A., and Kandlikar, S. G., 2020, "Transforming Pool Boiling into Self-Sustained Flow Boiling through Bubble Squeezing Mechanism in Tapered Microgaps," Appl. Phys. Lett., **116**(8), p. 081601.

[40] Kandlikar, S. G., 2022, "Microscale to Macroscale—Extending Microscale Enhancement Techniques to Large-Scale Boiling Equipment," Journal of Heat Transfer, **144**(5).

[41] Gorenflo, D., Chandra, U., Kotthoff, S., and Luke, A., 2004, "Influence of Thermophysical Properties on Pool Boiling Heat Transfer of Refrigerants," International Journal of Refrigeration, **27**(5), pp. 492–502.

[42] Peng, H., Ding, G., Hu, H., and Jiang, W., 2011, "Effect of Nanoparticle Size on Nucleate Pool Boiling Heat Transfer of Refrigerant/Oil Mixture with Nanoparticles," International Journal of Heat and Mass Transfer, **54**(9), pp. 1839–1850.

[43] Inoue, T., Monde, M., and Teruya, Y., 2002, "Pool Boiling Heat Transfer in Binary Mixtures of Ammonia/Water," International Journal of Heat and Mass Transfer, **45**(22), pp. 4409–4415.

[44] Liang, G., and Mudawar, I., 2018, "Review of Pool Boiling Enhancement with Additives and Nanofluids," International Journal of Heat and Mass Transfer, **124**, pp. 423–453.

[45] Taylor, R. A., and Phelan, P. E., 2009, "Pool Boiling of Nanofluids: Comprehensive Review of Existing Data and Limited New Data," International Journal of Heat and Mass Transfer, **52**(23), pp. 5339–5347.

[46] Wen, D. S., and Wang, B. X., 2002, "Effects of Surface Wettability on Nucleate Pool Boiling Heat Transfer for Surfactant Solutions," International Journal of Heat and Mass Transfer, **45**(8), pp. 1739–1747.

[47] Chi-Yeh, H., and Griffith, P., 1965, "The Mechanism of Heat Transfer in Nucleate Pool Boiling—Part II: The Heat Flux-Temperature Difference Relation," International journal of heat and mass transfer, **8**(6), pp. 905–914.

[48] Kandlikar, S. G., 2017, "Enhanced Macroconvection Mechanism With Separate Liquid–Vapor Pathways to Improve Pool Boiling Performance," Journal of Heat Transfer, **139**(5).

[49] Mikic, B. B., and Rohsenow, W. M., 1969, "A New Correlation of Pool-Boiling Data Including the Effect of Heating Surface Characteristics," Journal of Heat Transfer, **91**(2), pp. 245–250.

[50] Moore, F. D., and Mesler, R. B., 1961, "The Measurement of Rapid Surface Temperature Fluctuations during Nucleate Boiling of Water," AIChE Journal, **7**(4), pp. 620–624.

[51] Webb, R. L., 1981, "Performance Evaluation Criteria for Use of Enhanced Heat Transfer Surfaces in Heat Exchanger Design," International Journal of Heat and Mass Transfer, **24**(4), pp. 715–726.

[52] Ahammed, N., Asirvatham, L. G., and Wongwises, S., 2016, "Thermoelectric Cooling of Electronic Devices with Nanofluid in a Multiport Minichannel Heat Exchanger," Experimental Thermal and Fluid Science, **74**, pp. 81–90.

[53] Khan, M. G., and Fartaj, A., 2011, "A Review on Microchannel Heat Exchangers and Potential Applications," International Journal of Energy Research, **35**(7), pp. 553–582.

[54] Sheikholeslami, M., and Ganji, D. D., 2016, "Heat Transfer Enhancement in an Air to Water Heat Exchanger with Discontinuous Helical Turbulators; Experimental and Numerical Studies," Energy, **116**, pp. 341–352.

[55] Webb, R. L., and Trauger, P., 1991, "How Structure in the Louvered Fin Heat Exchanger Geometry," Experimental Thermal and Fluid Science, **4**(2), pp. 205–217.

[56] Zheng, N., Liu, P., Shan, F., Liu, Z., and Liu, W., 2016, "Effects of Rib Arrangements on the Flow Pattern and Heat Transfer in an Internally Ribbed Heat Exchanger Tube," International Journal of Thermal Sciences, **101**, pp. 93–105.